PCCP

Accepted Manuscript

ROYAL SOCIETY OF CHEMISTRY

www.rsc.org/pccp

Monitoring the intramolecular charge transfer process in the Z907 solar cell sensitizer: A transient VIS and IR spectroscopy and ab-initio investigation

Nicolò Azzaroli[1], Maria Grazia Lobello[2], Andrea Lapini[1,3,4], Alessandro Iagatti[1,4], Laura Bussotti[1], Mariangela Di Donato[1,3,4], Giuseppe Calogero[5], Mariachiara Pastore*[2], Filippo De Angelis[2], Paolo Foggi[1,4,6]*

1 *European Laboratory for Non Linear Spectroscopy (LENS), Università di Firenze, via Nello Carrara 1, 50019 Sesto Fiorentino, Florence, Italy*

2 *Computational Laboratory for Hybrid Organic Photovoltaics (CLHYO), Istituto CNR di Scienze e Tecnologie Molecolari, Via Elce di Sotto 8, I-06123 Perugia, Italy*

3 *Dipartimento di Chimica "Ugo Schiff", Universita' di Firenze, via della Lastruccia 13, 50019 Sesto Fiorentino (FI), Italy*

4 *INO-CNR, Istituto Nazionale di Ottica – Consiglio Nazionale delle Ricerche, Largo Fermi 6, 50125 Florence, Italy*

5 *CNR-IPCF, Istituto per i Processi Chimico-Fisici, Via F. Stagno D'Alcontres 37,98158 Messina, Italy*

6 *Dipartimento di Chimica, Biologia e Biotecnologie, Università di Perugia, Via Elce di Sotto 8, 06123 Perugia, Italy*

e-mail: iagatti@lens.unifi.it; chiara@thch.unipg.it

Abstract

We have analyzed the excited state dynamics of the heteroleptic [$(NCS)_2Ru(bpy\text{-}(COOH)_2)(bpy\text{-}(C_6H_{13})_2)$] Z907 solar cell sensitizer in solution and its interfacial electron transfer properties when adsorbed on thin TiO_2 films, by combining transient visible and infrared (IR) spectroscopies with ab initio Density Functional Theory (DFT) and Time-Dependent DFT (TDDFT) calculations. Upon excitation with ultra-short pulses in ethanol and dimethyl-sulphoxyde solutions, the visible spectra show the appearance of a positive signal around 650 nm, within the instrumental time resolution (<100 fs), which in ethanol undergoes a red-shift in about 20 ps. Measurements in the IR indicate that, upon excitation, both the CN and CO marker bands, associated to the NCS and COOH groups, downshift in frequency, in response to intramolecular ligand+metal (Ru-NCS) to ligand' (bpy-$COOH_2$) charge transfer (LML'CT). Vibrational cooling is observed in both solvents; in ethanol it is overtaken by the hydrogen bond dynamics. On the basis of DFT/TDDFT calculations, explicitly modeling the interaction of the NCS and COOH groups with solvent (ethanol) molecules, we rationalize the observed IR and visible spectral evolution as arising from the change in the Hydrogen-bond network, which accompanies the transition to the lowest-energy triplet state. This interpretation provides a consistent explanation of what observed also in the transient visible spectra. Transient IR measurements repeated for molecules adsorbed on TiO_2 and ZrO_2 films, allow us to identify the structural changes signaling the dye triplet excited state formation and evidence multiexponential electron injection rates into the semiconductor TiO_2 film.

1. Introduction

Dye-sensitized solar cells (DSSCs) have attracted notable interest in the last few years as effective low-cost devices for solar energy conversion.[1, 2] In these systems a dye molecule, adsorbed on a nano-crystalline thin-film semiconductor through a molecular bridge, harvests solar energy and transfers electrons into the semiconductor conduction band (CB). The oxidized dye is then regenerated by the electrolyte, usually based on the iodide/triodide redox couple, which closes the circuit allowing current flow across the device.[3] An essential feature of these solar cells is a large effective surface area for light absorption, which allows for the fabrication of thin-film semiconductor devices, facilitating efficient charge separation across the interface and lowering the fabrication costs for the semiconductor layer. In the last 20 years diverse classes of molecules of different chemical nature, such as metal complexes,[4, 5] porphyrines[6-8] or organic push-pull dyes,[9-11] have been designed and characterized to be used as efficient sensitizers for DSSCs. Essential characteristics of an ideally highly efficient dye sensitizer are: i) high absorption coefficient; ii) long term stability; iii) high yield

of photoinduced interfacial electron transfer into the semiconductor CB; and iv) relatively slow charge recombination dynamics.

Ruthenium(II) polypyridine complexes have been widely employed in dye sensitized solar cells, with solar to electric power efficiencies exceeding 11%.[8, 12, 13] In these dyes, the charge injection into the semiconductor CB can occur in principle directly via the initially excited singlet charge transfer state, though the occurrence of an ultrafast intersystem crossing (ISC) process, characteristic of this class of compounds, usually favors the injection of the electron from the lowest triplet state.[14] The nature of the low-lying electronic transitions in these systems is ~~in~~ of ligand+metal to ligand' charge transfer (LML'CT) character, with ligands such as CN and NCS increasing the absorption strength and tuning the wavelength of the visible transitions.[15-17] The interfacial electron transfer process in ruthenium polypiridyl complexes has been widely investigated by means of ultrafast spectroscopic techniques both in the visible and infrared (IR) spectral ranges.[3] In the IR, the thiocyanate CN stretching modes provide a useful probe to follow the intramolecular and interfacial CT processes following the electronic excitation: they have, in fact, well isolated and intense vibrational bands whose frequency is very sensitive to the charge density change. The carboxylic moieties, introduced on the bipyridyne ligands to graft the dye on the TiO_2 surface, provide an additional IR marker positioned in the acceptor part of the molecule, which is useful to follow the dynamics of charge injection and recombination.[18] Previous studies on the charge injection dynamics for the most efficient N3 and N719 Ru(II) dyes have revealed the occurrence of multi-exponential interfacial electron injection towards the polycrystalline TiO_2 semiconductor, revealing both an ultrafast (<100 fs) phase and slower picosecond component(s).[3] These results are usually interpreted in terms of a two state mechanism: the fast component is attributed to ultrafast injection from the non-thermalized initially excited ^{1}LML'CT state, while the slower phase represents injection from the equilibrated ^{3}LML'CT state, reached in these system on a sub-ps time scale, thus competing with initial electron transfer from the singlet state. Injection from the triplet state is strongly multi-exponential, presenting different phases with time constants spanning from tens to hundreds of picoseconds.[19-21] The reasons for this marked multi-exponentiality have been ascribed to various factors, such as heterogeneity of the TiO_2 film,[22] different electron coupling between the surface and photosensitizer, depending on the multiple ways in which the molecule can be adsorbed onto the semiconductor film or nanoparticle,[21] formation of dye aggregates on the semiconductor,[23] interligand electron transfer within the sensitizer.[24]

To rationalize the excited state sensitizer dynamics and to deeply understand the relation between the sensitizer structure and its efficiency, it is necessary to have a precise knowledge of both the excited states energies and the photodynamics. Also, the comparison of the excited state deactivation pathways of the dye when adsorbed on a semiconductor surface with those recorded in solution can

often deliver additional information. With this aim, here we study the dynamics of excited state relaxation of the widely used Z907 [$(NCS)_2Ru(bpy\text{-}(COOH)_2)(bpy\text{-}(C_6H_{13})_2)$] bipyridine-Ru(II) sensitizer(see Scheme 1).[25-29]

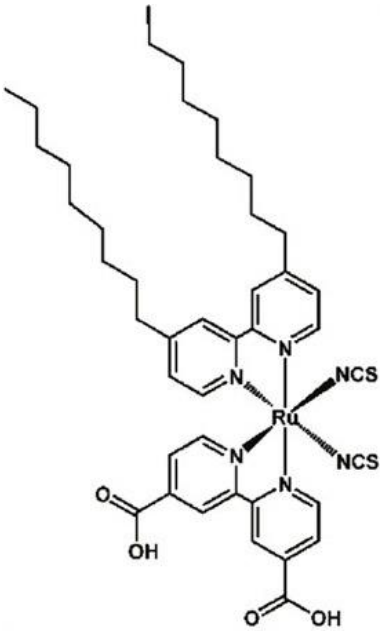

Scheme 1. Molecular structure of the Z907 sensitizer.

In this molecule, one of the two bipyridine ligands has a modified structure, with attached two dinonyl chains. Previous studies indicated that this chemical modification has the effect of increasing the stability of the oxidized form of the molecule and reduce its degradation in water environments with respect to similar dyes such as N3 and N719.[4, 30]

We have analyzed the excited state behavior of Z907 in protic and non protic solvents, namely ethanol (EtOH) and dimethyl-sulphoxyde (DMSO), employing ultrafast transient spectroscopy in the visible and Mid-IR spectral ranges. Furthermore, using transient IR spectroscopy, we have analyzed the behavior of this molecule when adsorbed on a non-conductive ZrO_2 surface. Finally, we have studied the dynamics of electron injection into a TiO_2 polycrystalline film. The reported experimental measures have been complemented with a theoretical analysis, based on DFT and TDDFT calculations, addressed to characterize the IR and UV-Vis response of the molecule both in protic and non protic solvents. By modeling the explicit interaction of one solvent (EtOH) molecule with each NCS and COOH group, we have interpreted the observed spectral IR evolution of both the CO and CN markers as arising from the change in the hydrogen bond network, which follows the electronic excitation from the ground to the lowest-energy triplet state, also providing a consistent explanation of what observed in the transient visible spectra. Our results, in fact, indicate a strengthening/weakening of the hydrogen bond between the COOH/NCS groups and the ethanol

molecules as a consequence of the movement of electronic charge from the thiocyanate to the carboxylic moieties. Furthermore, transient IR measurements of interfacial electron injection into the TiO_2 surface confirm the presence of an ultrafast (<100 fs) dynamic phase and of multiple slower ps components, in agreement with previous observation made for the structurally similar N3 and N719 dyes.[3]

2 Materials & methods

Sample preparation

Z907 dye powders (Dyesol) were purified before measurements by using HPLC (Waters 996, equipped with a photodiode array detector). The dye powder was solubilized in EtOH and injected in the cromatographic column (Phenomenex Jupiter, 10 μm, C18, 250 mm × 21 mm). The mobile phase consisted of distilled acetonitrile with 0.1% of trifluoroacetic acid (CF_3COOH).[31]The powders were dissolved in EtOH and DMSO, with concentrations of ~10^{-5} for visible and ~10^{-4} M for transient IR measurements. Solvents of spectroscopic grade were purchased from Sigma-Aldrich and used without further purification.

For transient IR measurements the spectral cell consisted of two 2-mm calcium fluoride windows separated by a 50 μm Teflon spacer. The cell was mounted on a home-made movable sample holder to minimize sample degradation and multiple excitation. For visible transient absorption the sample solution was contained in a 2-mm quartz cuvette. Magnetic stirring with a small magnet directly inserted into the cuvette ensured sample refreshing during data acquisition.

Dye-sensitized substrates were obtained by immersion in a ≈10^{-4}M solution in EtOH for at least 12 hours followed by repeated rinsing with EtOH and complete drying in air.

The semiconductor substrates (ZrO_2 or TiO_2) were prepared as follows. The ZrO_2 nanoparticles suspension was fabricated by the following a procedure similar to that of preparation of TiO_2 by sol gel technique.[32]

10 ml of Zirconium iso-propoxide were injected into 5.5g of glacial acetic acid under argon atmosphere and stirred for 10 minutes. The mixture was then injected into 50 ml of 0.1 M nitric acid under anhydrous atmosphere at room temperature in a flask and stirred vigorously. The flask was left uncovered and heated at 90°C for 8 hours. After cooling, the solution was filtered using a 0.45 μm syringe filter, diluted to 5% wt. ZrO_2 by the addition of H_2O and then autoclaved at 220°C for 12 hours. The ZrO_2 colloids solution was then concentrated to 10% on a rotary evaporator using a membrane vacuum pump at a temperature at 40ºC. Carbowax 20,000 (Aldrich) was added and the resulting paste was stirred slowly overnight to ensure homogeneity.[33] Otherwise, for the TiO_2 films a commercial screen printing paste (Dyesol 18NRT) was employed.

Each suspension was spread on the substrates by a glass rod, using 3M adhesive tapes as spacers. After the films were dried in air, they were sintered at 450°C for 20 minutes in air. The thickness of the as prepared films was controlled using different tapes, resulting in film thicknesses of 3-4 μm.[34] The thickness of the oxide film deposited on the photoanodes was measured by using a DektakXT profilometer (Bruker) equipped with a diamond-tipped stylus (radius of 2μm) and selecting a vertical scan range of 65 μm with 8.0 nm resolution and a stylus force of 1 mg. Each measure was verified by acquiring different runs, starting from different positions set by rotating or translating the sample.

Ultrafast measurements

UV-Vis Transient Absorption spectroscopy (TAS) experiments have been widely described in previous papers.[35] The fs-laser oscillator is a Ti:sapphire laser (Spectra Physics Tsunami) pumped by the second harmonic from a Nd:YVO (Spectra Physics Millennia). The short (≤70 fs) pulses are stretched and amplified at 1 kHz repetition rate by a regenerative amplifier (BMI Alpha 1000). After compression a total average power of 450-500 mW and pulse duration of 100 fs are obtained. The repetition rate of the output beam is reduced to 100 Hz by a mechanical chopper in order to avoid the photodegradation of the sample.

The 520 nm pump pulses (energy reduced at 100 nJ/pulse) are obtained by Sum Frequency Generation (SFG) of the signal output of an optical parametric amplifier (TOPAS by Light Conversion, Vilnius, Lithuania) with a portion of the laser fundamental output at 800 nm. The polarization angle between pump and probe beams is adjusted at 54.7° so as to exclude rotational contributions to the transient signal. Multichannel detection for transient spectroscopy was achieved by sending the white light continuum after passing through the sample to a flat field monochromator coupled to a home-made CCD detector.[http://lens.unifi.it/ew]

Femtosecond visible-pump/Mid-IR probe experiments are performed using the set-up previously described.[36] About 20% of the output of a regenerative amplified Ti:sapphire oscillator system (Coherent Legend Elite, 810 nm central wavelength, 1 KHz rep. rate, pulse energy > 3 mJ/pulse, 35 fs pulse duration) is employed for the experiment. A fraction (~70 μJ/pulse) of the output is directed to a home-built Non-Collinear Optical Parametric Amplifer (NOPA), producing tunable visible-light pulses in the 450-700 nm range. For the present experiment the bandwidth is reduced to approximately 60 nm and centered at 520 nm with energy/pulse around 500nJ.

A second portion (~300 μJ per pulse) of the 810 nm fundamental is used to pump a home-built OPA producing near-IR pulses; difference frequency of idler and signal is finally generated in 1 mm thick $AgGaS_2$ crystal providing tunable pulses in the Mid-IR region. Around $\lambda = 6$ μm, spectrally broad pulses (typical bandwidth > 200 cm^{-1}) are obtained with energy of about 1 μJ and duration of ~150

fs. A fraction (4-5%) of the Mid-IR output passes through a half-wave plate controlling the polarization and is used as the source of probe and reference beams in the experiment. The probe and reference beams, of equal intensity, are obtained by reflection from the faces of a wedged CaF_2 plate and focused onto the sample by a parabolic mirror. Both probe and reference beams are sent to a flat-field monochromator and imaged onto a double 32-channel array Mercury Cadmium Telluride (MCT) infrared detector.

The infrared probe has been tuned to monitor spectral changes in both the CN and CO absorbing region, respectively centered around 2100 and 1700 cm^{-1}. All measurements have been performed at room temperature. The integrity of the samples has been checked by Uv-Vis absorption (Lambda900) and FTIR (Bruker Alpha-T) before and after the ultrafast measurements.

Data analysis

The quantitative analysis of the data obtained by the ultrafast transient visible absorption and transient IR experiments has been performed using a combined approach consisting of singular values decomposition (SVD) and global fitting. Both steps are performed using the GLOTARAN package.[37] The number of kinetic components has been defined through the SVD procedure. The following parameterization of the time evolution of the relative intensities and of the associated spectral contributions (evolution associated decay spectra, EADS) has been performed adopting a unidirectional sequential model with increasing lifetimes.

Computational details

To properly model the ground and the excited state vibrational and visible spectra and their changes as a consequence of the hydrogen bond network modifications, we optimized the molecular structure of i) protonated dye (Z907), ii) protonated dye with two EtOH molecules interacting with the -NCS ligands (hereafter indicated as **Z907+2EtOH_NCS**, Figure 1A) and iii) protonated dye with two EtOH molecules interacting with the -COOH groups (hereafter indicated as **Z907+2EtOH_COOH**, Figure 1B) both in the ground (GS) and triplet excited state (T). The geometry optimizations and the corresponding frequencies calculations were performed using B3LYP[38] exchange-correlation (xc) functional, a 3-21G* basis set, this being a well-assessed protocol for the characterization of Ru-based metal complexes.[13, 39] The implicit solvent-solute interactions, for both EtOH and DMSO, where modeled using the C-PCM[40] approach as implemented in the Gaussian 09 (G09) program package.[41] Excited state calculations on the isolated Z907 in EtOH and DMSO as well as on the

Z907+2EtOH_COOH/ Z907+2EtOH_CN adducts in EtOH were carried out with the B3LYP xc functional and the DGDZVP basis set [42]

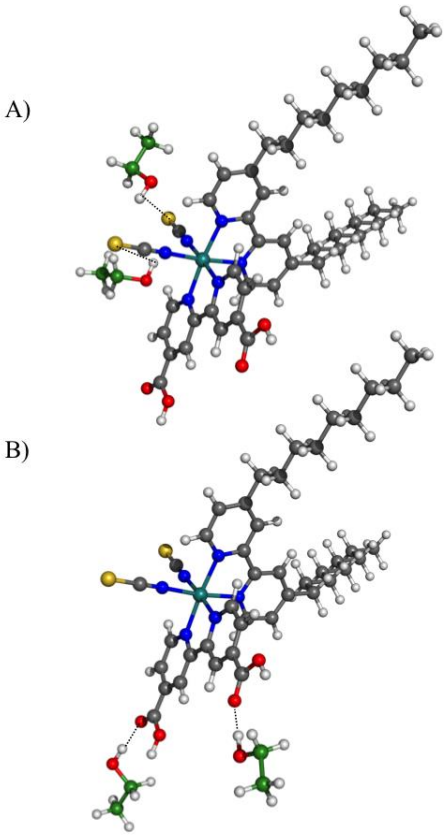

Figure 1. Ground state optimized molecular structure of A) **Z907+2EtOH_SCN** and B) **Z907+2EtOH_COOH**. Carbon atoms of EtOH are in green.

3 Results and discussion

3.1 Ultrafast Visible Measurements in solution

The TAS spectra measured for Z907 in EtOH and DMSO are reported in Figure 2 at different pump-probe delay times.

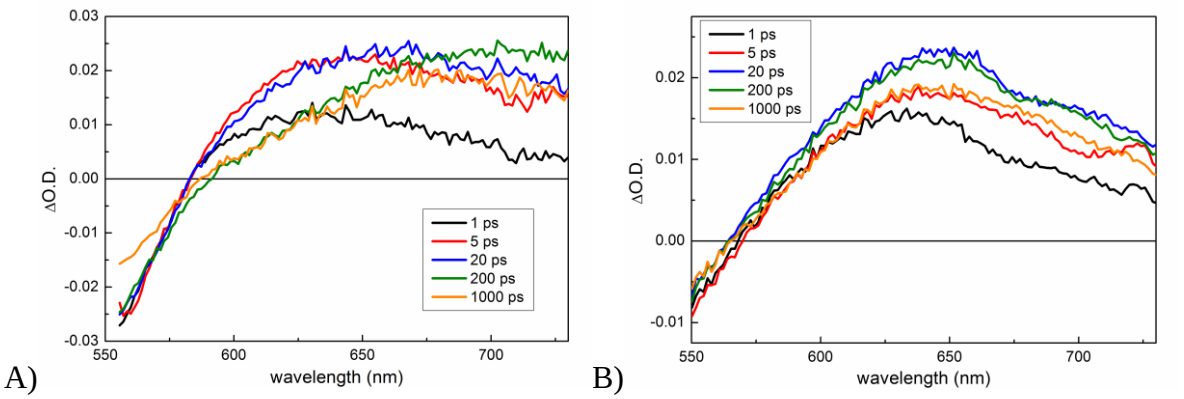

Figure 2. (A) UV/Vis Transient absorption spectra of Z907 upon excitation at 520 nm in A) EtOH and B) DMSO solution.

The spectra in both solvents are characterized by the onset of the negative signal due to the ground state bleaching (minimum at 520 nm masked by a cut-off filter) and by a broad positive excited absorption signal (ESA) in the range 600-750 nm which was ascribed to the long lived triplet ^{3}LML'CT transition.[3, 20] The excited state triplet absorption appears on an ultrafast timescale, below the instrument time resolution, confirming the occurrence of intersystem crossing from the initially excited ^{1}LML'CT on a <100 fs timescale, as previously reported for this molecule and similar systems.[3] The subsequent spectral evolution is notably different in the two analyzed solvents. While in DMSO only a minor band-shape change is observed on a few picosecond timescale, a significant red-shift is noted in EtOH, occurring on a 20-30 ps timescale. The evolution of the transient absorption spectra is better visualized by observing the EADS obtained by global analysis of the data, shown in Figure 3.

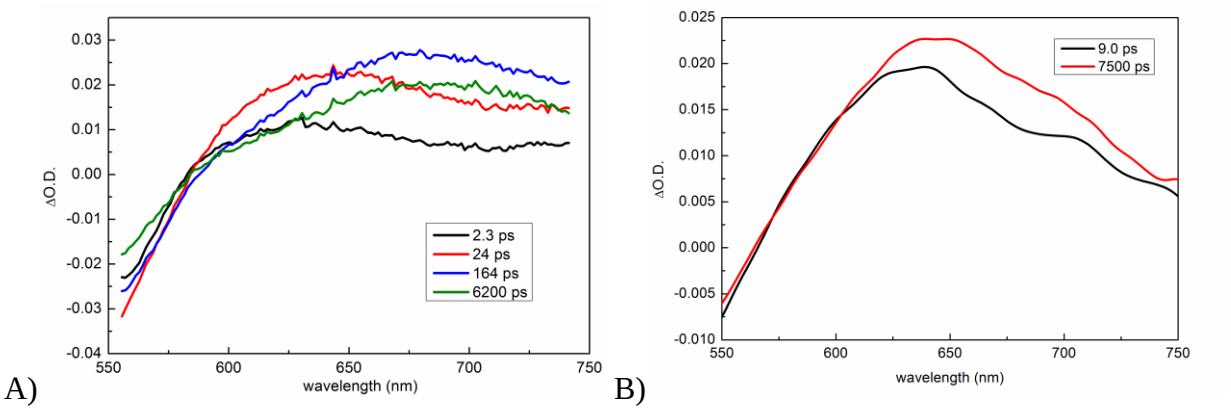

Figure 3. EADS obtained from global analysis of the transient absorption data recorded for the Z907 dye upon excitation at 520 nm in A) EtOH and B) DMSO solution. Normalized EADS are shown in the inset of each panel.

In EtOH four different time components are necessary to properly fit the data, while only two time constants are sufficient in case of the DMSO solution. The fit procedure shows a good convergence, with residual error values <0.003 in both cases. The interpretation of the excited state evolution in DMSO is quite straightforward: upon the ultrafast formation of the ^{3}LML'CT state, occurring on a <100 fs timescale, intramolecular vibrational relaxation occurs on a 9-10 ps timescale, followed by ground state recovery on a timescale longer than the interval probed within our measurements. In a protic medium like EtOH additional dynamics, possibly connected with hydrogen-bond rearrangement, is observed. Global fit of the kinetic traces in this solvent retrieves two ps components: the first 2.4 ps component results in an increased intensity of the ^{3}LML'CT excited state absorption band, while the following 24 ps component is associated to a 20 nm red-shift of the same band. Although no significant spectral change is associated with the following 164 ps component, a decay component on this timescale is clearly visible for kinetic traces at wavelength >650 nm (see Figure S1 in the Supporting Information (SI)). Similarly a small shift of the maximum of the broad feature around 700 nm is observed in the first 500 ps, possibly associated to solvent induced relaxation. The relaxation dynamics of alcohol such EtOH shows, in fact, a component in the hundreds of picosecond interval.[43] The determination of the long time decay lifetime suffers from a relatively higher error than that associated to the shorter lifetimes, due to the limited time window probed within our measurement.

3.2 Ultrafast transient IR measurements in solution

In order to further investigate the relaxation dynamics of Z907 in solution we performed ultrafast infrared measurements, probing both the CO and the CN absorption regions, in EtOH and in DMSO The latter solvent has been chosen for its high polarizabilty and its capability to form hydrogen bond acting only as a proton acceptor. Thanks to these properties DMSO should react faster than EtOH to the solute charge redistribution.[43] In the excited state both the CO and CN bands downshift as a consequence of the intramolecular charge transfer. Upon visible light absorption electron density moves from the isothiocyanate towards the bipyridine ligands, which determines a downshift of the CO absorption frequency, due to the increased charge density accumulating on the molecular moiety on which these functional groups are located. Concerning the thiocyanates, upon charge transfer from the ruthenium center towards the bipyridine ligands, their electronic structure can be predominantly

seen as [Ru:N$^{(-)}$=C=S], where the CN stretching is expected to absorb at lower frequencies compared with the absorption of the [Ru:N≡C-S$^{(-)}$] structure prevailing in the ground state.

Figure 4 reports the EADS obtained by globally fitting the kinetic traces recorded in the CO absorption region (centered around 1670 cm^{-1}) in the two analyzed solvents, selected time resolved spectra are reported in the SI (Figure S4).

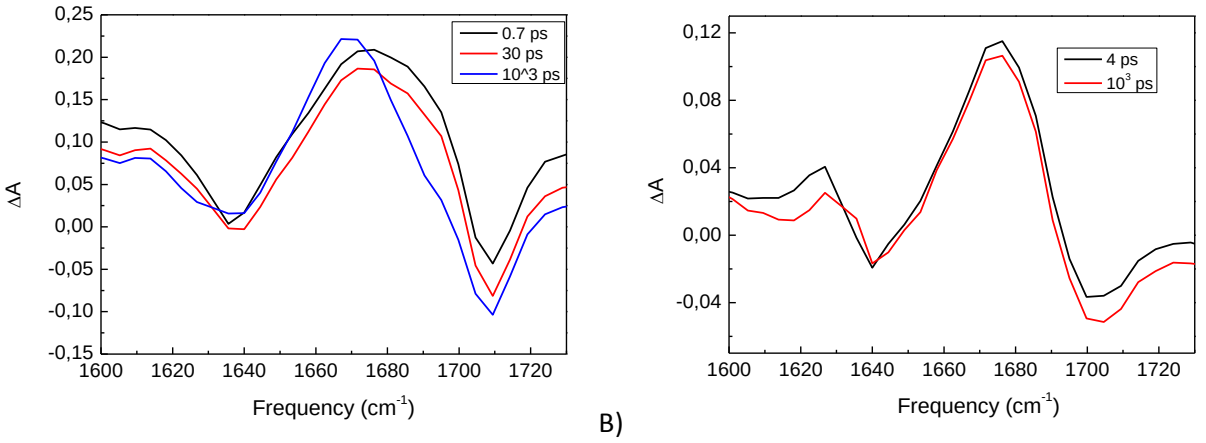

Figure 4. Evolution associated decay spectra obtained by global analysis of the IR transient data referring to the CO absorption region in A) EtOH, B) DMSO

As it can be noticed, the spectral evolution in the CO region is markedly different in the two analyzed solvents. As already observed from TAS measurements, three kinetic components are necessary to correctly fit the transient data recorded in EtOH solution, while only two time constants are sufficient in case of DMSO. The lifetimes obtained in the infrared are comparable with those obtained in the visible. In EtOH the CO stretching absorption initially downshifts from 1710 cm^{-1} in the ground state to 1675 cm^{-1}. The excited state absorption band is initially very broad and unstructured and undergoes a small narrowing and intensity change on a ~1 ps timescale. Following this fast evolution, which could be due to fast relaxation in the non-thermalized ultrafast formed ^{3}LML'CT, we observe a significant narrowing and a further 5 cm^{-1} red-shift of the band, occurring on a 30 ps timescale. Finally the system relaxes to the ground state on a long timescale, not accessible within our time measuring window. In the non-protic DMSO, the evolution is much simpler and no significant band shape change or band shifts are observed. The 4 ps lifetime obtained from global analysis can be interpreted in terms of vibrational relaxation on the readily formed ^{3}LML'CT state.

The EADS obtained by globally fitting the data recorded in the CN absorption region (centered around 2050 cm^{-1}) are reported in Figure 5, selected time resolved spectra are reported in the SI for both ETOH and DMSO (Figure S5).

The spectral evolution in the CN region again shows a different behavior in the two solvents.

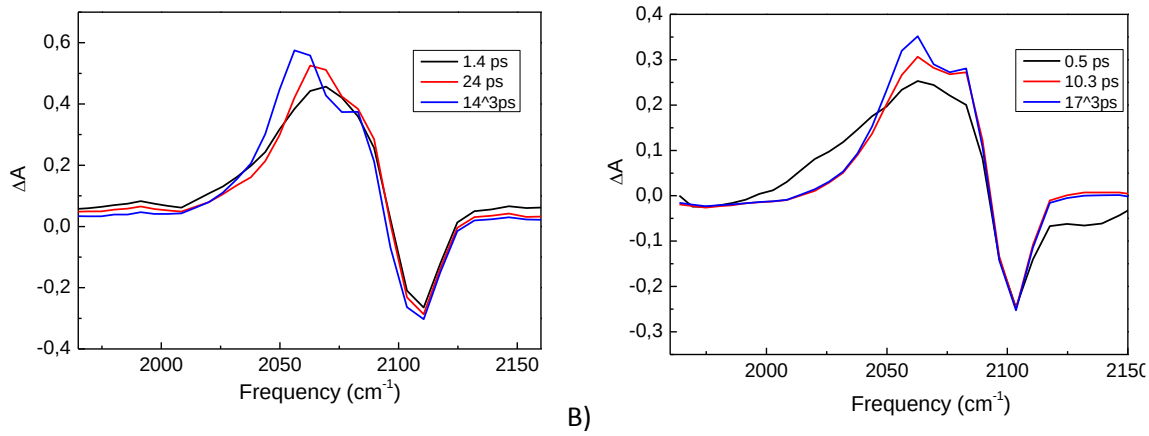

Figure 5. Evolution associated decay spectra obtained by global analysis of the IR transient data referring to the CN absorption region in A) EtOH, B) DMSO

A single peak due to ground state bleaching is observed at 2107 cm^{-1} in EtOH (2103 cm^{-1} DMSO), which has been assigned to both symmetric and antisymmetric CN stretching.[44] At the excited state the CN absorption moves to lower frequencies and in both solvent a double peak structure develops on a few picosecond timescale. The two bands observed on the long timescale at 2056 and 2083 cm^{-1} in EtOH (2062 and 2083 cm^{-1} in DMSO) can be attributed to the symmetric and antisymmetric CN stretching, whose absorption maxima are more separated in the excited state due to an increased vibrational coupling among these two modes caused by the electronic redistribution following the LML'CT transition.

In EtOH the CN excited state absorption band is initially very broad, peaking 2070 cm^{-1} and undergoes a significant narrowing on a 1.4 ps timescale. Based on the results of a recent 2D IR study executed on the analogous N3 dye, this dynamic phase can be attributed to vibrational energy redistribution among the symmetric and antisymmetric CN stretchings.[45] Following this initial evolution, the excited state band becomes more structured, leading to the appearance of a clear double peak on a 24 ps timescale, with the lower frequency peak downshifted with respect to the initial central frequency. The timescale of this evolution is similar to that previously determined both from visible transient absorption and in the CO absorption region in the same solvent. Since a dynamic evolution on a comparable timescale is not observed in DMSO we attribute it to solvent reorganization involving hydrogen-bond dynamics. In DMSO the spectral evolution is rather limited. A double peak structure in the CN excited state absorption develops on a 0.5 ps timescale, but at later times only a modest band narrowing on a 10 ps time scale is observed, which can be attributed to vibrational cooling. Finally, on a long timescale (behind our measuring time) ground state is recovered, but no spectral shift is observed.

3.3 Computational analyses

On the basis of the results of all the transient measurements reported above and the differences observed in protic and non protic solvents, here we shall derive a theoretical framework to explain the dynamics observed for Z907 in solution, by modeling the IR and UV-Vis response in different environments.

Notice that similar combinations of theoretical tools and IR spectroscopy were recently employed to characterize weak intermolecular interactions in complex biological systems.[46]

The excitation at 520 nm brings population to the excited ^{1}LML'CT that relaxes on an ultrafast time scale on the ^{3}LML'CT, meaning that the charge redistribution within the metal complex is extremely fast and the solvent molecules do not have the time to re-equilibrate their charge and hydrogen-bond distances in such a fast time. As we shall discuss, the subsequent dynamics is thus dominated by solvent relaxation and hydrogen-bond strengthening/weakening in case of EtOH, in response to the mutated electronic distribution in the different functional groups of the molecule As a matter of fact, in our calculations we cannot simulate the weakening/strengthening of the hydrogen bonds, as we can only reproduce the equilibrium situations that to say: i) the **Z907+2EtOH_COOH** (or **Z907+2EtOH_NCS**) adduct (see structures in Figure 1), with stable hydrogen-bonds; ii) the Z907 dye alone

Upon excitation, negative charge flows towards the bipyridine ligands, yielding a charge depletion on the thiocyanate ligands and charge accumulation on the carboxylic groups (see the HOMO-LUMO density difference plot in Figure 6). According to this charge redistribution it can be reasonably hypothesized a weakening of the EtOH-NCS hydrogen-bonds accompanied by a strengthening of the EtOH-OCOH interactions.

The analysis of the Z907-EtOH adducts in the ground and in the triplet states at equilibrium geometries provides us indications about the rearrangement of the solvent molecules upon excitation. As shown by the binding energies and the hydrogen-bonds distances reported in Table 1, in the **Z907+2EtOH_SCN** adduct, the interaction becomes weaker (the distance longer) going from the ground state to the triplet, in agreement with the calculated charge depletion on the ligands in the excited state (see Mulliken charge values listed in Table 2). On the contrary in the **Z907+2EtOH_COOH** adduct, upon excitation, as a consequence of the increased charge on the COOH groups (Table 1), the hydrogen-bond becomes markedly stronger, with a gain of more than 10 kcal/mol in the binding energy of the Z907-EtOH complex.

Table 1. Calculated hydrogen bonds distances (in Å) and Z907-EtOH adducts binding energies (kcal/mol) at the ground state (S0) and excited state (T1) equilibrium geometries.

H-bond distances (Å)		
System	S0	T1
Z907+2EtOH_NCS_1/NCS_2	2.38/2.38	2.44/2.43
Z907+2EtOH_COOH_1/COOH_2	1.80/1.80	1.74/1.76
Binding Energy (kcal/mol)		
System	S0	T1
Z907+2EtOH_NCS	23.51	22.05
Z907+2EtOH_COOH	7.13	18.49

Table 2. Mulliken charges for the thiocyanate and carboxylic groups.

Group	S0	T1
NCS_1	-0.70	-0.57
NCS_2	-0.70	-0.56
COOH_1	-0.03	-0.11
COOH_2	-0.04	-0.13

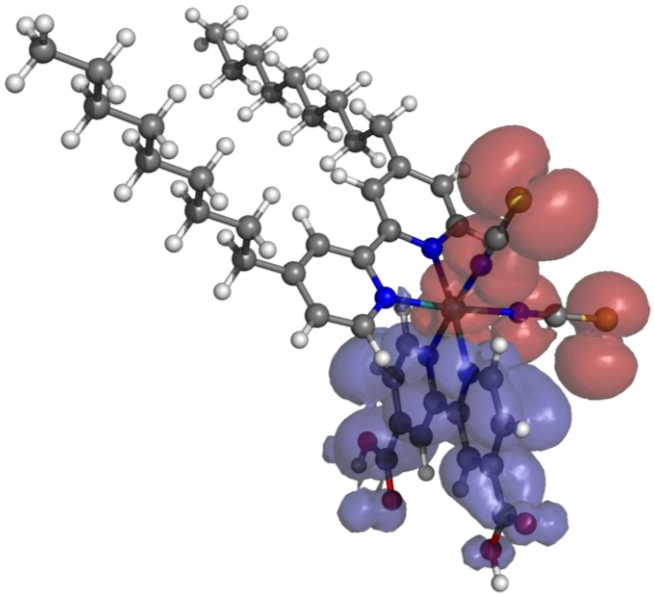

Figure 6. Isodensity plots of the HOMO-LUMO density difference of the Z907 complex. Red/blue lobes correspond to charge depletion/accumulation.

The comparison between the calculated and experimental differential IR spectra is plotted in Figure 7A) and 7B) for the CO and CN stretching, respectively; note that, for an easier visual evaluation, the position of the ground state bleaching in the simulated spectra was shifted so to agree to that of the experimental ones. Furthermore, to highlight the effect of the explicit solvent molecules in the excited state, we shifted the relative position of the simulated spectra for the Z907 with and without the explicit solvent in way to align the bleaching position in the two cases.

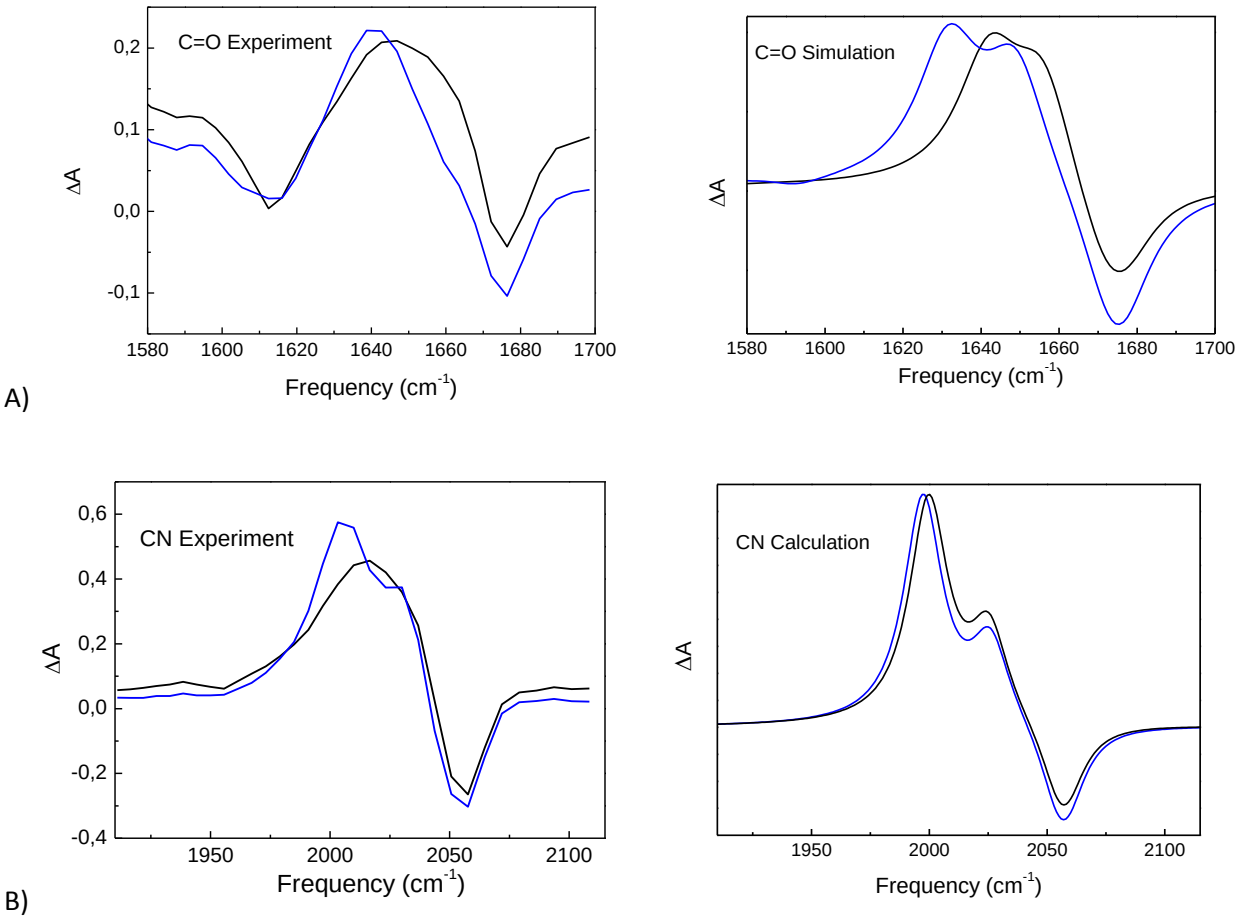

Figure 7. A) Comparison between experimental and calculated transient IR spectra in the A) CO and B) CN absorption region. In the left panel of figure 6A) and 6B) black/blue lines are the short/long leaving EADS component shown in Figures 4A) and 5A).

As expected on the basis of the indications obtained by the calculated bond distances and adduct binding energies, we reproduced the spectral shift in the CO stretching (Figure 7A), where the hydrogen-bond is supposed to be reinforced in the triplet state, by simulating the early times neglecting the solute-solvent interaction (Z907 alone, black line), and the longer times by computing

the IR spectrum of the **Z907+2EtOH_COOH** adduct (blue line). As it can be noticed, the model is able to nicely reproduce the measured spectral modifications, predicting a red-shift of 36 cm^{-1} to be compared to that experimentally determined of 9 cm^{-1}. The overestimation of the calculated spectral shift is, however, not surprising, since our picture is considering the two limit cases in the hydrogen-bond formation/breaking. In the case of the CN stretching, where upon excitation the hydrogen bonds are supposed to become weaker, we simulate the early times with the **Z907+2EtOH_NCS** adduct (black line in Figure 7B), whereas longer delay times with the isolated dye (blue line in Figure 7B). The calculated spectra qualitatively reproduce the observed evolution: the excited state red-shift of the CN absorption is well reproduced, as well as the observed relative intensity change of the two excited state absorption band on a long timescale.

In order to highlight the differences between the protic and non protic solvents examined in this work we also simulated the transient infrared spectra for Z907 in DMSO. The results are reported in SI (Figure S5) for both the CO and CN regions, where it is shown that the calculated spectra well reproduce the excited state downshift of both the CO and CN absorptions observed in the experiments. Furthermore the calculated UV-Vis absorption spectra in both solvents are reported in SI (Figure S6).

3.4 Electron injection dynamics on TiO_2

Besides studying the dynamics of Z907 in solution we have also monitored both the behavior of the molecule when adsorbed on a non-conductive ZrO_2 substrate and the electron injection dynamics into the TiO_2 CB. The measurements for the sample adsorbed on both solid substrates have been conducted without covering the sample with any solvent, but keeping it under dry nitrogen flux during the measurement. We have analyzed the systems by transient infrared spectroscopy, probing the CN absorption region. The EADS obtained by a global fit of the data measured for Z907 adsorbed on ZrO_2 are reported in Figure 8, together with the kinetic trace at 2055 cm^{-1} and the relative fit.

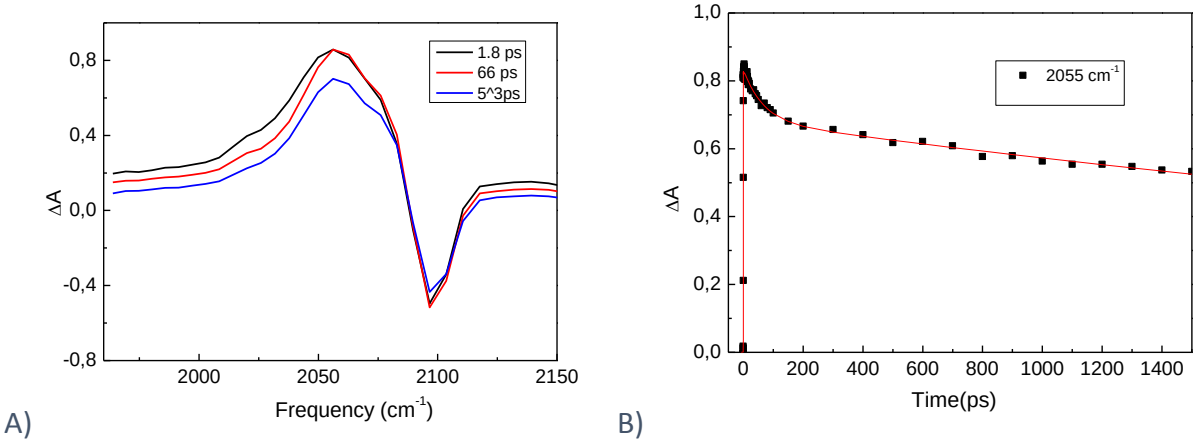

Figure 8. A) Evolution associated decay spectra obtained by globally analyzed the IR transient data referring to the CN absorption region of Z907 adsorbed on zirconia. B) kinetic trace at 2055 cm^{-1} (scattered points) and fit obtained from global analysis (red line).

As it can be noticed from Figure 8, the CN stretching absorbs at slightly lower frequency in the ground state when the molecule is adsorbed on the ZrO_2 substrate with respect to both the analysed solvents, indicating a slight weakening of the CN bond possibly due to a higher degree of charge localization on the bipyridine molecular moiety coordinated to the surface. In the excited state the CN absorptions shift to lower frequency, as expected because of the reduced CN bond order following the LML'CT transition. Contrarily to what observed in solution, the symmetric and antisymmetric stretching are not well separated and a broad excited state band is observed, peaking at 2056 cm^{-1}. Only a weak shoulder at 2076 cm^{-1} can be resolved. The dynamic evolution of the signal is very limited: the excited state absorption band slightly sharpens on a 1.8 ps timescale, probably reflecting vibrational population equilibration among the two CN groups[45] and successively decays by about 20% on a 66 ps timescale, as it can clearly be noticed by inspecting the kinetic trace reported in Figure 8B. The decay of the excited state absorption band is not accompanied by a comparative bleaching recovery. The intensity of the latter signal is almost unchanged during the time interval probed by our measurement, indicating only minimal ground state recovery. Although injection into the ZrO_2 CB is prevented due to the high band gap of this material (~5 eV), electron transfer is possible towards surface states, whose energy is below that of the CB. This process has been observed for several bypiridyl metal complexes and organic dyes, and is favoured when a quite strong coupling between the dye and the surface is established.[44, 47-50] In our case, the observed shift of the CN absorption band suggests that coordination with the ZrO_2 surface can induce a charge localization on the coordinating bipyridine moiety, favouring the formation of charge transfer states. Furthermore, if electron transfer to surface states is operative in Z907 adsorbed on ZrO_2 charge recombination could also be observed.

In case of several organic dyes substantial signal decrease has been observed on a nanosecond time scale, due to back electron transfer from the ZrO_2.[48, 50] In our system we only notice a slight recovery of the bleaching signal, which could be due to charge recombination from trap or defect surface states. When Z907 is adsorbed on a TiO_2 substrate, the typical broad absorption due to free electrons injected in the semiconductor CB is observed in the probed Mid-IR region, as shown in Figure 9. Superimposed to the electron signal, bleaching and excited state absorption of the CN groups are also observed. By inspecting the kinetic traces in the analysed IR region, as that at 2150 cm^{-1} reported in Figure 9B, it is possible to notice that almost 70% of the signal rises on a time scale <100 fs, thus below our instrument time resolution.

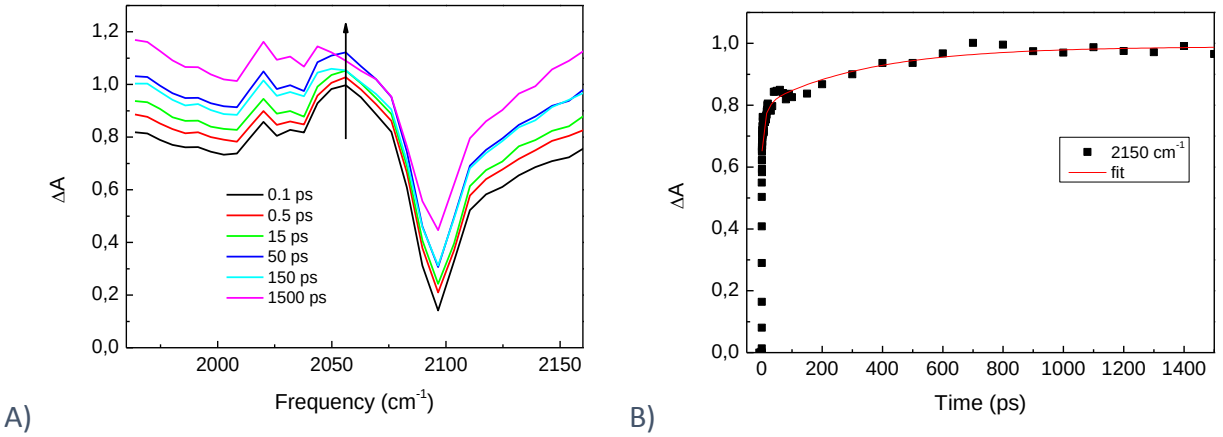

Figure 9. A) Selected transient spectra of Z907 adsorbed on Titania referring to the CN absorption region. B) kinetic trace at 2150 cm^{-1} (scattered points) and relative fit (red line)

By fitting the kinetic traces in the region where no absorption bands of the molecule are observed, it is possible to retrieve the electron injection kinetics into the TiO_2 CB. As it can be noticed the electron injection is markedly multi-exponential. Fitting the kinetic trace reported in Figure 9B, by excluding the initial 500 fs, and considering that 70% of the injection occurs on a time scale <100 fs, gives time components of 0.6 ps (15%), 15 ps (6%) and 325 ps (9%). Similar picosecond injection components have been reported for other Ruthenium-bipyridine dyes such as N3 and N719 and ascribed to injection from the thermalized ^{3}LML'CT state.[3, 20, 51] The time constants of the slower injection dynamics from the long living triplet state show a high degree of variability among the previously conducted studies.[3] It has been shown that the longer time constants are highly dependent on the experimental conditions, such as excitation wavelength and excitation power, presence of trap states into the semiconductor as well as on sample preparation and degradation.[21] Also, the presence of electrolytes such as I^-/I_3^- can affect the long-time component of the electron injection, because of a stabilizing effects on the dye cation, as it has been recently shown.[52] In case of our measurements,

the longer injection components of 15 and 325 ps could also be ascribed to formation of aggregates or the presence of differently-oriented adsorbed molecules (Z907 has a bulky substituent on one of the bipyridines which could cause more heterogeneous absorption) or to partial sample degradation.

4. Conclusions

We have investigated the excited state relaxation dynamics of the Z907 dye in two different solvents using both transient visible and infrared spectroscopy. Upon excitation with visible light ultrafast intersystem crossing from the initially excited ^{1}LML'CT state occurs, with a time constant comparable with our instrumental time resolution (<100 fs). The following dynamics can be rationalized in terms of vibrational cooling in the promptly formed ^{3}LML'CT state. In a protic solvent like EtOH additional slow dynamics is observed on a 30 ps time scale, which has been interpreted in terms of hydrogen bond rearrangement on the basis of the experimental observation and DFT/TDDFT calculations. The analysis of the injection dynamics in the mid-IR spectral range confirms a two state electron transfer mechanism previously proposed for similar dyes N3 and N719. Upon light absorption, electrons are injected for almost 70% on an ultrafast time scale (<100 fs) from the initially excited non thermalized ^{1}LML'CT. Triplet formation competes with this fast injection dynamics. The following slower picosecond injection components occur from the relaxed triplet state. Electron transfer from the ^{3}LML'CT is highly multi-exponential, as previously reported for similar molecules.

Acknowledgments

The authors gratefully acknowledge the financial support from the Italian MIUR: program FIRB "Futuro in Ricerca 2010" grant RBFR10Y5VW to M.D.D. and RBFR109ZHQ supporting A.L., project CNR-EFOR L. 191/2009 art. 2 comma 44. The research leading to these results has received also funding from LASERLAB-EUROPE (grant agreement no. 284464, EC's Seventh Framework Programme). MGL, FDA and MP thank MIUR-PRIN 2010-2011 Project No. 20104XET32 "DSSCX".

References

1 B. O'Regan and M. Gratzel, *Nature*, 1991, **353**, 737-740.

2 A. Hagfeldt, G. Boschloo, L. Sun, L. Kloo and H. Pettersson, *Chem. Rev.*, 2010, **110**, 6595-6663.

3 N. A. Anderson and T. Q. Lian, in *Annu. Rev. Phys. Chem.*, Annual Reviews, Palo Alto, 2005, vol. 56, pp. 491-519.

4 A. Fattori, L. Peter, K. McCall, N. Robertson and F. Marken, *J.Solid State Electr.*, 2010, **14**, 1929-1936.

5 M. Pellnor, P. Myllyperkiö, J. Korppi-Tommola, A. Yartsev and V. Sundström, *Chem. Phys. Lett.*, 2008, **462**, 205-208.

6 L.-L. Li and E. W.-G. Diau, *Chem. Soc. Rev.*, 2013, **42**, 291-304.

7 A. Yella, H.-W. Lee, H. N. Tsao, C. Yi, A. K. Chandiran, M. K. Nazeeruddin, E. W.-G. Diau, C.-Y. Yeh, S. M. Zakeeruddin and M. Grätzel, *Science*, 2011, **334**, 629-634.

8 G. Calogero, A. Bartolotta, G. Di Marco, A. Di Carlo and F. Bonaccorso, *Chem. Soc. Rev.*, 2015, **44**, 3244-3294.

9 W. Zeng, Y. Cao, Y. Bai, Y. Wang, Y. Shi, M. Zhang, F. Wang, C. Pan and P. Wang, *Chem. Mater.*, 2010, **22**, 1915-1925.

10 N. Zhou, K. Prabakaran, B. Lee, S. H. Chang, B. Harutyunyan, P. Guo, M. R. Butler, A. Timalsina, M. J. Bedzyk, M. A. Ratner, S. Vegiraju, S. Yau, C.-G. Wu, R. P. H. Chang, A. Facchetti, M.-C. Chen and T. J. Marks, *J. Am. Chem. Soc.*, 2015, **137**, 4414-4423.

11 C. Koenigsmann, T. S. Ripolles, B. J. Brennan, C. F. A. Negre, M. Koepf, A. C. Durrell, R. L. Milot, J. A. Torre, R. H. Crabtree, V. S. Batista, G. W. Brudvig, J. Bisquert and C. A. Schmuttenmaer, *Phys. Chem. Chem. Phys.*, 2014, **16**, 16629-16641.

12 M. K. Nazeeruddin, A. Kay, I. Rodicio, R. Humphry-Baker, E. Mueller, P. Liska, N. Vlachopoulos and M. Graetzel, *J. Am. Chem.l Soc.*, 1993, **115**, 6382-6390.

13 M. Pastore, A. Selloni, S. Fantacci and F. De Angelis, in *First Principles Approaches to Spectroscopic Properties of Complex Materials*, Springer Berlin Heidelberg, 2014, vol. 347, pp. 1-45.

14 N. H. Damrauer, G. Cerullo, A. Yeh, T. R. Boussie, C. V. Shank and J. K. McCusker, *Science*, 1997, **275**, 54-57.

15 S. Campagna, F. Puntoriero, F. Nastasi, G. Bergamini and V. Balzani, in *Photochemistry and Photophysics of Coordination Compounds I*, ed. V. Balzani and S. Campagna, Springer Berlin Heidelberg, 2007, vol. 280, pp. 117-214.

16 S. Fantacci, F. De Angelis and A. Selloni, *J. Am. Chem. Soc.*, 2003, **125**, 4381-4387.

17 V. Balzani, A. Juris, M. Venturi, S. Campagna and S. Serroni, *Chem. Rev.*, 1996, **96**, 759-834.

18 P. Paoprasert, J. E. Laaser, W. Xiong, R. A. Franking, R. J. Hamers, M. T. Zanni, J. R. Schmidt and P. Gopalan, *J. Phys. Chem. C*, 2010, **114**, 9898-9907.

19 Y. Tachibana, J. E. Moser, M. Gratzel, D. R. Klug and J. R. Durrant, *J. Phys. Chem.,* 1996, **100**, 20056-20062.

20 G. b. Benko, J. Kallioinen, J. E. I. Korppi-Tommola, A. P. Yartsev and V. Sundström, *J. Am. Chem. Soc.*, 2002, **124**, 489-493.

21 J. B. Asbury, N. A. Anderson, E. Hao, X. Ai and T. Lian, *J. Phys. Chem. B*, 2003, **107**, 7376-7386.

22 Y. Tachibana, I. V. Rubtsov, I. Montanari, K. Yoshihara, D. R. Klug and J. R. Durrant, *J. Photoch. Photobio. A*, 2001, **142**, 215-220.

23 B. Wenger, M. Gratzel and J.-E. Moser, *J. Am. Chem. Soc.*, 2005, **127**, 12150-12151.

24 J. Kallioinen, G. b. Benkö, P. Myllyperkiö, L. Khriachtchev, B. Skårman, R. Wallenberg, M. Tuomikoski, J. Korppi-Tommola, V. Sundström and A. P. Yartsev, *J. Phys. Chem. B*, 2004, **108**, 6365-6373.

25 P. Wang, S. M. Zakeeruddin, J. E. Moser, M. K. Nazeeruddin, T. Sekiguchi and M. Grätzel, *Nat. Mater.*, 2003, **2**, 402-407.

26 R. Jiang, A. Anderson, P. R. F. Barnes, L. Xiaoe, C. Law and B. C. O'Regan, *J. Mater. Chem. A*, 2014, **2**, 4751-4757.

27 S. M. Zakeeruddin, M. K. Nazeeruddin, R. Humphry-Baker, P. Pechy, P. Quagliotto, C. Barolo, G. Viscardi and M. Grätzel, *Langmuir*, 2002, **18**, 952-954.

28 E. Mosconi, J.-H. Yum, F. Kessler, C. J. Gòmez Garcìa, C. Zuccaccia, A. Cinti, M. K. Nazeeruddin, M. Grätzel and F. De Angelis, *J. Am. Chem. Soc.*, 2012, **134**, 19438-19453.
29 T. Moehl, H. N. Tsao, K.-L. Wu, H.-C. Hsu, Y. Chi, E. Ronca, F. De Angelis, M. K. Nazeeruddin and M. Grätzel, *Chem. Mater.*, 2013, **25**, 4497-4502.
30 S. M. Zakeeruddin, M. K. Nazeeruddin, R. Humphry-Baker, P. Péchy, P. Quagliotto, C. Barolo, G. Viscardi and M. Grätzel, *Langmuir*, 2002, **18**, 952-954.
31 P. Salvatori, G. Marotta, A. Cinti, C. Anselmi, E. Mosconi and F. De Angelis, *J. Phys. Chem. C*, 2013, **117**, 3874-3887.
32 M. Grätzel, *J. Sol-Gel Sci. Techn.*, 2001, **22**, 7-13.
33 C. S. Kim and H. D. Jeong, *Bull. Korean Chem. Soc.*, 2007, **28**, 2333-2337.
34 G. Calogero, J.-H. Yum, A. Sinopoli, G. Di Marco, M. Grätzel and M. K. Nazeeruddin, *Sol. Energy*, 2012, **86**, 1563-1575.
35 P. L. Gentili, L. Bussotti, R. Ruzziconi, S. Spizzichino and P. Foggi, *J. Phys. Chem. A*, 2009, **113**, 14650-14656.
36 N. Azzaroli, A. Lapini, M. Di Donato, A. Dei and R. Righini, *J. Phys. Chem. B*, 2013, **117**, 15492-15502.
37 J. J. Snellenburg, S. Laptenok, R. Seger, K. M. Mullen and I. H. M. van Stokkum, *J. Stat. Softw.*, 2012, **49**, 1-22.
38 A. D. Becke, *J. Chem.l Phys.*, 1993, **98**, 1372-1377.
39 S. Fantacci and F. De Angelis, *Coordin. Chem. Rev.*, 2011, **255**, 2704-2726.
40 M. Cossi, N. Rega, G. Scalmani and V. Barone, *J. Comput. Chem.*, 2003, **24**, 669-681.
41 M. J. Frisch and e. al, Gaussian 09, Gaussian, Inc, Wallingford CT, 2009.
42 N. Godbout, D. R. Salahub, J. Andzelm and E. Wimmer, *Can. J. Chemistry*, 1992, **70**, 560-571.
43 M. Maroncelli and G. R. Fleming, *J. Chem.l Phys.*, 1987, **86**, 6221-6239.
44 J. B. Asbury, R. J. Ellingson, H. N. Ghosh, S. Ferrere, A. J. Nozik and T. Lian, *J. Phys. Chem. B*, 1999, **103**, 3110-3119.
45 M. Fedoseeva, M. Delor, S. C. Parker, I. V. Sazanovich, M. Towrie, A. W. Parker and J. A. Weinstein, *Phys. Chem. Chem. Phys.*, 2015, **17**, 1688-1696.
46 R. Chaudret, B. de Courcy, J. Contreras-Garcia, E. Gloaguen, A. Zehnacker-Rentien, M. Mons and J. P. Piquemal, *Phys. Chem. Chem. Phys.*, 2014, **16**, 9876-9891.
47 S. Verma, P. Kar, A. Das, D. K. Palit and H. N. Ghosh, *J. Phys. Chem. C*, 2008, **112**, 2918-2926.
48 K. Oum, O. Flender, P. W. Lohse, M. Scholz, A. Hagfeldt, G. Boschloo and T. Lenzer, *Phys. Chem. Chem. Phys.*, 2014, **16**, 8019-8029.
49 K. Oum, P. W. Lohse, O. Flender, J. R. Klein, M. Scholz, T. Lenzer, J. Du and T. Oekermann, *Phys. Chem. Chem. Phys.*, 2012, **14**, 15429-15437.
50 R. Huber, S. Spörlein, J. E. Moser, M. Grätzel and J. Wachtveitl, *J. Phys. Chem. B*, 2000, **104**, 8995-9003.
51 G. Benkö, J. Kallioinen, P. Myllyperkiö, F. Trif, J. E. I. Korppi-Tommola, A. P. Yartsev and V. Sundström, *J. Phys. Chem. B*, 2004, **108**, 2862-2867.
52 D. Di Tommaso, E. Ruiz-Agudo, N. H. de Leeuw, A. Putnis and C. V. Putnis, *Phys. Chem. Chem. Phys.*, 2014, **16**, 7772-7785.

Graphical Abstract